ACS OMEGA

Open Access

http://pubs.acs.org/journal/acsodf

Article

Chemical Structure Characteristics and Model Construction of Coal with Three Kinds of Coalification Degrees

Chengyong Wang,* Yaowen Xing, Kaiyi Shi, Shiwei Wang, Yangchao Xia, Jihui Li, and Xiahui Gui

Cite This: *ACS Omega* 2024, 9, 1881−1893

Read Online

ACCESS | Metrics & More | Article Recommendations

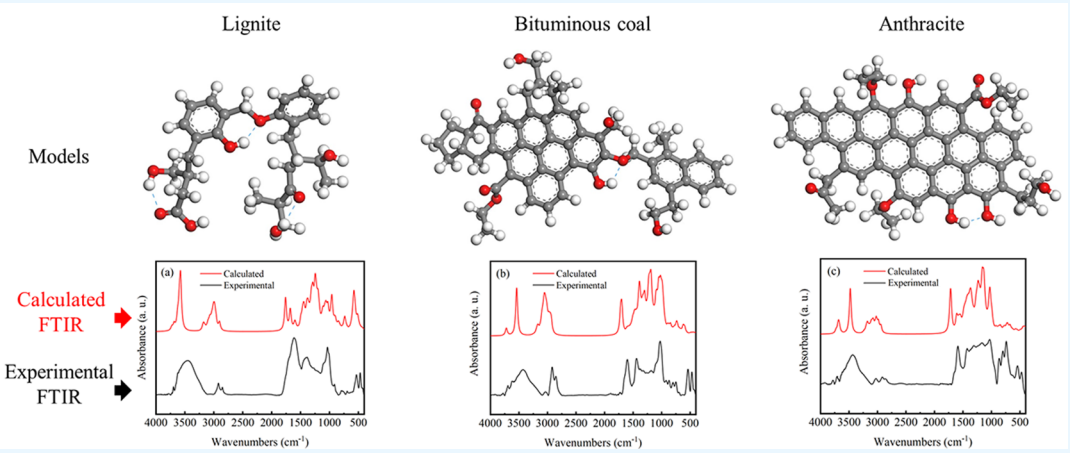

ABSTRACT: The coal structure is extensively used for studying the properties of coal, and the construction of accurate and reliable coal structure models can promote these researches. In this study, Fourier transform infrared (FTIR) spectroscopy and X-ray diffraction (XRD) were used to analyze the changes in the coal structure as a function of the coalification degree, and a semiquantitative model construction method based on FTIR, XRD, and X-ray photoelectron spectroscopy (XPS) analyses was proposed. With an increase in the coalification degree, the size of the aromatic cores in the coal increased. During the conversion from lignite to bituminous coal, the content of aliphatic structures increased, while the content of oxygen-containing functional groups (OFGs) significantly decreased. Conversely, during the conversion from bituminous coal to anthracite, the content of aliphatic structures decreased while the content of OFGs slightly increased. The calculated FTIR spectra of the coal structure models were consistent with the experimental FTIR spectra, which confirmed the accuracy of the models. Furthermore, the models successfully explained the microscopic mechanism underlying the differences in the wettability of the coal samples with varying coalification degrees. The construction method and coal structure models in this study will be more widely applied in future research.

1. INTRODUCTION

The chemical structure of coal is one of the dominant factors influencing the wettability,[1,2] calorific value,[3,4] chemical reactivity,[5,6] and cohesiveness[7] of coal, which have a significant impact on its industrial processing and conversion. Therefore, a deep understanding of the coal structure can help realize the highly efficient utilization of coal. A range of physical or chemical analytical methods have been used to study the coal structure, and many well-known structure models have been developed, such as the Shinn model,[8] Given model,[9,10] Faulon model,[11,12] Wender model,[13] and Wiser model.[14] It is widely accepted that coal is composed of many basic structural units with similar but not identical structures. These structural units are made up of regular condensed polycyclic aromatic hydrocarbons and irregular aliphatic chains, functional groups, and bridge bonds.[15,16]

With the advancement of new instrument-based analytical techniques, coal structure research is becoming more sustainable and in-depth. Some information regarding the coal structure may be obtained using FTIR, XRD, XPS, solid-state ^{13}C nuclear magnetic resonance (^{13}C NMR) spectrosco-

Received: October 30, 2023
Revised: December 5, 2023
Accepted: December 7, 2023
Published: December 27, 2023

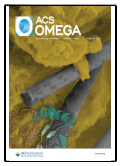

py, and high-resolution transmission electron microscopy (HRTEM) without having to destroy the coal molecules.[17−21] Kawashima et al.[22] made some correction to the model structures of Upper Freeport coal extracts using ^{13}C NMR spectra. Wang et al.[17] constructed a structure model of lignite obtained from Inner Mongolia using XRD, ^{13}C NMR, HRTEM, and XPS, and verified the model by comparing the calculated FTIR spectrum of the model and the measured FTIR spectrum. Feng et al.[23] obtained key information regarding the coal molecules using ^{13}C NMR, XPS, and FTIR analyses. A structure model of the coal was constructed using computer-aided modeling, and the model was optimized and further verified by the calculated FTIR and ^{13}C NMR spectra with quantum chemical calculations. Wang et al.[24] used ^{13}C NMR, FTIR, XPS, XRD techniques, and molecular modeling methods to establish the coal structure model of Qinghua coal.

The Wender model and Wiser bituminous model are extensively used in molecular simulations to study the properties of coal at the molecular/atomic level, since they can capture a number of fundamental aspects of coal structures with a low molecular weight, which can save computational resources during simulation.[25−29] Zhang et al.[26] performed molecular dynamics (MD) simulations to investigate the wettability of coal with varying coalification degrees. They employed the lignite and anthracite models proposed by Wender as well as the Wiser bituminous coal model. The findings showed that the simulated contact angles were in agreement with the experimental results. Guo et al.[25] studied the adsorption behavior of sodium dodecyl sulfonate (SDS) and dodecyl trimethylammonium bromide (DTAB) on the surface of lignite using MD simulation. The Wender model was utilized as the lignite model in the simulation. Chen et al.[28] explored the interactions between coal and kaolinite in water through a combination of experiments and molecular simulations. The Wiser model was employed as the bituminous coal model in the simulation. Zhao et al.[29] used the Wiser model for the grand canonical Monte Carlo and MD simulations to study the diffusion properties of CO_2 and CH_4 in coal.

The molecular structure of coal has not been defined due to the various coal-forming plants, environments, and coalification degrees. If existing molecular models are used without modification, it can be difficult to accurately express the molecular structural characteristics of the research object. Hence, this study proposes a simple method for constructing models of coal molecules based on the results of FTIR, XRD, and XPS analyses that conform to the molecular structure characteristics of the tested samples. These models were successfully used to explain the internal factors contributing to the differences in the wettability of the coal samples. The chemical structure model of coal constructed in this study may be utilized in molecular simulation to explain various coal features, and the model construction method can be used to construct chemical structure models of coal samples in many research.

2. EXPERIMENTAL DETAILS AND SIMULATION

2.1. Coal Samples. Three types of coal samples with different coalification degrees were used in the study: lignite, bituminous coal, and anthracite. Lignite and bituminous coal (coking coal) were collected from Guizhou, China, and anthracite was obtained from Ningxia, China. The results of the proximate, ultimate, XPS, and water contact angle (WCA) analyses of these samples had been reported in our previous research.[30] The WCA analysis results showed that the wettability of lignite was the strongest, while that of bituminous coal was the weakest. The wettability of anthracite was slightly stronger than that of bituminous coal.[30] The analysis results of XPS are shown in Figure 1. The bituminous coal has the highest relative content of C−C/C−H, while the lignite has the highest relative content of C−O, C═O, and O−C═O.[30]

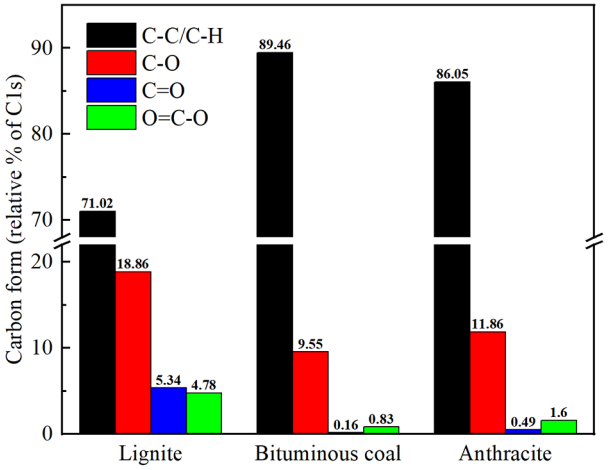

Figure 1. XPS analysis results of the coal samples.

2.2. FTIR Analysis. FTIR measurements of the coal samples were performed on an infrared spectrometer (Nicolet iS20, Thermo Scientific, USA). The samples were mixed with KBr in a mass ratio of 1:100, ground thoroughly, and then pressed into thin slices. FTIR spectra were recorded by coadding 32 scans with a resolution of 4.0 cm^{-1} and in a scan range of 400−4000 cm^{-1}. To thoroughly study the chemical structure, curve-fitting analyses were performed on the FTIR spectra using Origin software. Gaussian combination was used to determine the fitted peak shape and area, which were adjusted to minimize the variance between the experimental and fitted curves.

2.3. XRD Analysis. The data were obtained by using an X-ray polycrystalline diffractometer (LabX XRD-6100, Shimadzu, Japan) with Cu Kα radiation (40 kV, 30 mA). The scanning range and step size were set to 5°−80° and 0.02° (2θ), respectively. The XRD spectra were fitted to three Gaussian peaks at 2θ values of approximately 20°, 26°, and 43°, corresponding to the γ, (002), and (10) bands, respectively.[17,19,20]

2.4. Simulation Details. Density functional theory (DFT) calculations using the Dmol^3 module of Materials Studio software were performed to obtain the geometrically optimized structure, charge distribution, and vibrational frequency of the coal structure model. Additionally, the Vibration Analysis tool was utilized to simulate the FTIR spectra. The quality of the DFT calculations was set as fine. The exchange-correlation functional was Perdew−Wang 91 (PW91), and the basis set was the *d*-polarization functions (DNP). The energy, maximum force, and maximum displacement of the convergence tolerance were 1.0×10^{-5} Hartree, 0.002 Hartree/Å, and 0.005 Å, respectively.

https://doi.org/10.1021/acsomega.3c08574
ACS Omega 2024, 9, 1881−1893

3. RESULTS AND DISCUSSION

3.1. FTIR Analysis. *3.1.1. FTIR Spectra of Coal Samples.* The FTIR spectra of the coal samples can be divided into multiple zones, each corresponding to different types of functional groups.[18,31−35] As shown in Figure 2, the peaks in the 3600−3100 cm^{-1} zone can be assigned to the stretching vibration (υ) mode of the hydroxyl group (−OH) and hydrogen bond (HB) involving −OH. The 3000−2800 cm^{-1} zone shows peaks due to the υ mode of aliphatic structures. The peaks in the 1800−1000 cm^{-1} zone are complex and correspond to the υ mode of OFGs, such as carboxyl, ketones, ethers, alcohols, phenols, and esters; υ mode of aromatic C═C; deformation vibration (δ) mode of methyl ($-CH_3$) and methylene ($-CH_2-$); and υ mode of clay or silicate minerals Si−O−Si. The peaks in the 900−700 cm^{-1} zone can be assigned to the out-of-plane δ mode of aromatic C−H. In addition, the peaks in the 3100−3000 cm^{-1} zone can be assigned to the υ mode of aromatic C−H, and the peaks in the 600−400 cm^{-1} zone may be due to the δ mode of the alcohol hydroxyl group (R−OH).

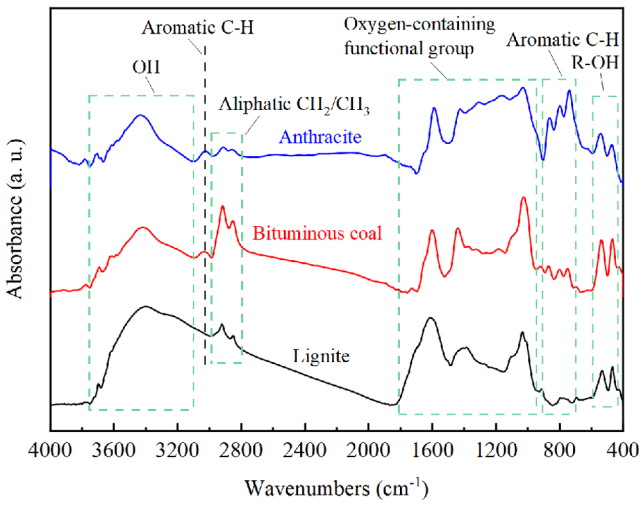

Figure 2. FTIR spectra of the coal samples.

As shown in Figure 2, the FTIR spectra of lignite, bituminous coal, and anthracite vary with the degree of coalification. The band of −OH (3600−3100 cm^{-1}) in bituminous coal and anthracite is significantly weaker than that in lignite, while in anthracite, it is slightly stronger than that in bituminous coal. This suggests that −OH and HB are more abundant in lignite but less so in bituminous coal and anthracite. The observed decrease in the −OH absorption band from lignite to bituminous coal can be assigned to a significant reduction in the content of −OH in the conversion process. During the conversion from bituminous coal to anthracite, the content of −OH in the coal showed a slight increase due to the reduction in the aliphatic structure and the condensation of the aromatic structure, leading to a minor change in the relative content of −OH in anthracite. The FTIR spectra analysis shows that the band of the aliphatic structure (3000−2800 cm^{-1}) in bituminous coal is the strongest,

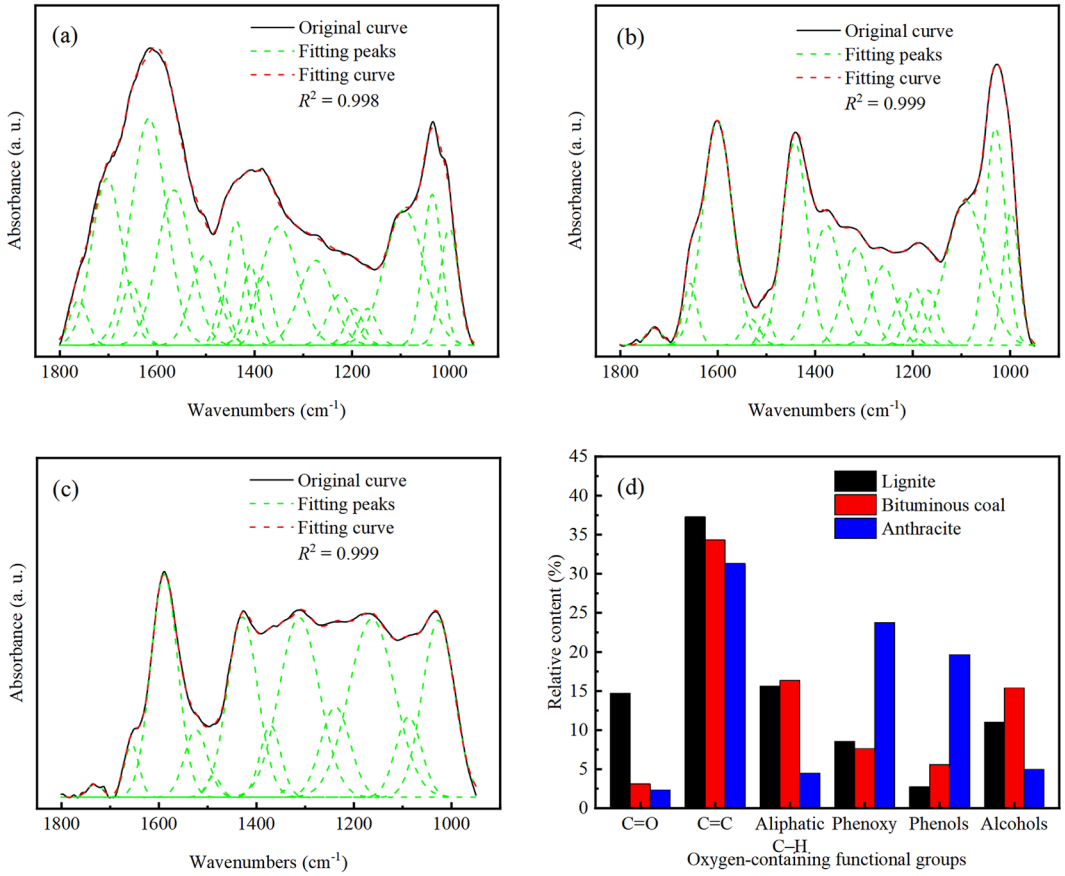

Figure 3. Curve-fitted FTIR spectra for the 1800−1000 cm^{-1} zone: (a) lignite, (b) bituminous coal, (c) anthracite, and (d) relative content.

https://doi.org/10.1021/acsomega.3c08574
ACS Omega 2024, 9, 1881−1893

followed by lignite, and last anthracite. This observation suggests that the content of aliphatic structures is highest in bituminous coal and lowest in anthracite. The weak reactivity of the aliphatic structures may be the reason for the lower cleavage during the conversion from lignite to bituminous coal. Additionally, the cleavage of the other functional groups may lead to an increase in the proportion of aliphatic structures or the generation of new aliphatic structures. However, during the conversion from bituminous coal to anthracite, the content of aliphatic structures decreased significantly due to the condensation of aromatic structures and aromatization of cycloalkanes. The stretching vibration peak (3100−3000 cm^{-1}) and aromatic structure absorption band (900−700 cm^{-1}) of the aromatic C−H in lignite, bituminous coal, and anthracite were successively enhanced. This is likely due to the continuous generation and condensation of the aromatic rings with an increasing degree of coalification. The band (1800−1000 cm^{-1}) of the OFGs was significantly weakened during the conversion from lignite to bituminous coal. The band (1300−1150 cm^{-1}) of anthracite was stronger than those of bituminous coal and lignite. This may be because the content of the aromatic ring in anthracite increased sharply, resulting in an increase in the contents of aromatic ether, phenolic hydroxyl, and other such functional groups.

3.1.2. Oxygen-Containing Functional Groups. Figure 3 shows the curve-fitted FTIR spectra for the 1800−1000 cm^{-1} zone. Table 1 presents the peak assignments. With the increase in the degree of coalification, the relative content of C═O decreased. The relative content of C═O in lignite (10.64%) was significantly higher than that in bituminous coal and anthracite. This is because lignite contains carboxyl, which is absent in bituminous coal and anthracite (there is no peak at 1700 cm^{-1} in Figure 3b,c). The slight decrease in the relative content of C═O during the conversion from bituminous coal to anthracite may be due to the decrease in the contents of aromatic esters and ketones. The relative contents of phenoxy (referring to aromatic ether and phenoxy) and phenols in anthracite were higher than those in lignite and bituminous coals. The relative content of phenols increased with the increase in the degree of coalification, while the phenoxy content remained relatively stable in lignite and bituminous coal. This may be due to the increase in the content of aromatic structures with the increase in the degree of coalification. During the conversion from bituminous coal to anthracite, the content of aromatic structures increased significantly, while the content of aliphatic structures decreased significantly (as shown in Figure 2). This resulted in an increased probability of the −OH and O atoms being connected to the aromatic structure. The relative content of alcohols increased during the conversion from lignite to bituminous coal but decreased during the conversion from bituminous coal to anthracite. This change is closely related to the change in the content of the aliphatic structures. The content of aliphatic structures increased during the conversion from lignite to bituminous coal, which increased the probability that −OH is connected with the carbon chains to form alcohols. However, during the conversion from bituminous coal to anthracite, the content of aliphatic structures significantly decreased and the probability of −OH and carbon chains forming alcohols decreased. Due to the changes in the relative content of various (OFGs), the proportion of the peak area corresponding to the stretching vibration of the aromatic C═C in this wavenumber range slightly decreased with the increase in the coalification degree.

Table 1. Assignment of Peaks in the 1800−1000 cm^{-1} Zone[18,36,37a]

Peak #	Position (cm^{-1})	Assignment[b]
1	1730	Aryl esters
2	1700	Carboxyl
3	1650	Ketone C═O
4	1618/1586/1502	Aromatic C═C
5	1458	δ_{as} mode of $-CH_3$, $-CH_2-$
6	1437	Aromatic C═C
7	1410	δ_{as} mode of α-CH_2
8	1377	δ_s mode of CH_3−Ar, R
9	1350	δ_s mode of CH_2−C═O
10	1274	υ mode of C−O in aryl ethers
11	1222	υ mode of C−O and δ of OH, phenoxy structure, ethers
12	1195/1168	υ mode of C−O phenols, ethers
13	1094	υ mode of C−O alcohols
14	1033/1009	υ mode of Si−O−Si

[a]Reprinted (Adapted or Reprinted in part) with permission from ref 18, an FTIR study of the evolution of coal structure during the coalification process. Copyright 1996 Elsevier Science Ltd. [b]δ: deformation vibration; υ: stretching vibration; as asymmetric; s: symmetric.

The functional groups containing C═O can be quantitatively characterized using the OFG parameter ($'C'$), which reflects the maturity of coal. The lower the value of $'C'$, the higher the maturity of coal. $'C'$ can be calculated using eq 1.[38−40]

$$'C' = \frac{A_{1800-1650}}{A_{1800-1650} + A_{1620-1500} + A_{1437}} \quad (1)$$

where $A_{1800-1650}$ corresponds to the area of the C═O band and $A_{1620-1500}$ and A_{1437} correspond to the areas of the aromatic C═C peaks. The $'C'$ values for lignite, bituminous coal, and anthracite were 0.28, 0.08, and 0.07, respectively. This indicates that with the increase in the coalification degree, the $'C'$ value decreases, signifying an increase in the maturity of coal. Furthermore, by taking the sum of the corresponding peak areas of the functional groups containing C−O (phenoxy, phenols, and alcohols) as 100%, it is possible to calculate the percentages of phenoxy, phenols, and alcohols, respectively. These parameters, as shown in Table 2, can be used to build coal structure models.

Table 2. Percentage of Phenoxy, Phenols, and Alcohols

	Percentage (%)		
Coal	Phenoxy	Phenols	Alcohols
Lignite	38.34	12.25	49.40
Bituminous coal	26.71	19.49	53.80
Anthracite	49.07	40.60	10.33

3.1.3. Aromatic Structures. Figure 4 shows that the 900−700 cm^{-1} zone can be divided into several peaks, respectively, corresponding to the C−H out-of-plane δ mode of the aromatic structures with one H atom (1H, 870 cm^{-1}), two adjacent H atoms (2H, 815 cm^{-1}), three adjacent H atoms (3H, 800 cm^{-1}), and four adjacent H atoms (4H, 750 cm^{-1}).[35,41,42]

https://doi.org/10.1021/acsomega.3c08574
ACS Omega 2024, 9, 1881−1893

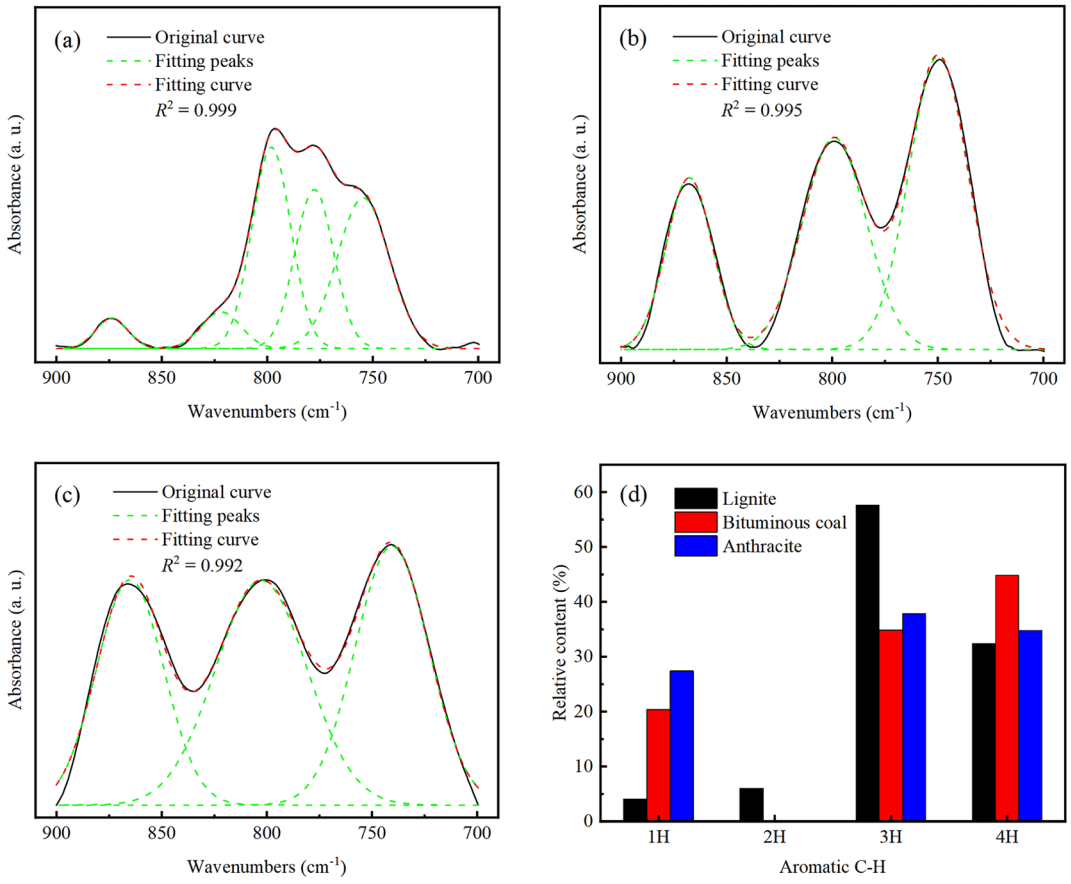

Figure 4. Curve-fitted FTIR spectra for the 900−700 cm^{-1} zone: (a) lignite, (b) bituminous coal, (c) anthracite, and (d) relative content.

The changes in the area of the peaks in the 900−700 cm^{-1} zone with the degree of coalification reflects the degree of substitution of the aromatic H atoms.[18,35,43] As shown in Figure 4d, lignite contains more 3H and 4H, while the relative content of 1H is low, indicating that the aromatic ring of lignite contains more H atoms and that the degree of condensation of the aromatic core is low. With the increase in the degree of coalification, the aromatic core condensed, thereby increasing the size of the aromatic cores and decreasing the number of adjacent aromatic H atoms. Therefore, the relative content of 1H increased, and the relative contents of 1H in bituminous coal and anthracite were significantly greater than that of 1H in lignite. The area ratio of the 1H peak to the 4H peak (aromatic structure parameter, *DOS*) can be used to quantify the degree of H atom substitution on the aromatic ring. *DOS* can be obtained using eq 2.[39,40]

$$DOS = \frac{A_{870}}{A_{750}} \tag{2}$$

where A_{870} and A_{750} correspond to the areas of the 1H and 4H peaks, respectively. The *DOS* values of lignite, bituminous coal, and anthracite were 0.12, 0.45, and 0.79, respectively. This indicates that the degree of substitution of the H atoms in the aromatic ring and the size of the aromatic cores increased with the increase in the degree of coalification degree.

3.1.4. Aliphatic Structures. The 3000−2800 cm^{-1} region can be divided into six peaks, as shown in Figure 5. The peaks are assigned to the $-CH_3$, $-CH_2-$ asymmetric υ mode (CH_3-as, CH_2-as) near 2950 and 2920 cm^{-1}, the $-CH_3$, $-CH_2-$ symmetric υ mode (CH_3-ss, CH_2-ss) near 2870 and 2850 cm^{-1}, and the methylene C−H υ mode (Machine C−H) near 2895 cm^{-1}.[35,41,43] The peak near 2830 cm^{-1} has been reported in other studies; however, its assignment has not been determined.[18,43]

Figure 5d shows the relative contents of the aliphatic structure. During the conversion from lignite to bituminous coal, the relative content of $-CH_3$ decreased (both the relative contents of CH_3-as and CH_3-ss decreased), while the relative content of $-CH_2-$ increased (the relative content of CH_2-as did not change significantly, while the relative content of CH_2-ss increased), which may be mainly due to the aliphatic chain cyclization and $-CH_3$ shedding. During the conversion from bituminous coal to anthracite, aromatization of cycloalkanes occurred and sharp condensation of the aromatic cores led to shortening of the aliphatic chain. Therefore, the relative content of $-CH_2-$ decreased, while the relative content of $-CH_3$ increased. The methylene content increased during the conversion from lignite to bituminous coal, while it did not change significantly during the conversion from bituminous coal to anthracite. Its relative content may be mainly affected by aliphatic chain cyclization and changes in the relative contents of $-CH_3$ and $-CH_2-$. The ratio of the peak areas (CH_2/CH_3) of 2920 cm^{-1} (CH_2−as) and 2950 cm^{-1} (CH_3-as) can reflect the length and degree of branching of the aliphatic chain.[38,39] CH_2/CH_3 can be calculated using eq 3.[38−40]

$$\frac{CH_2}{CH_3} = \frac{A_{2920}}{A_{2950}} \tag{3}$$

https://doi.org/10.1021/acsomega.3c08574
ACS Omega 2024, 9, 1881−1893

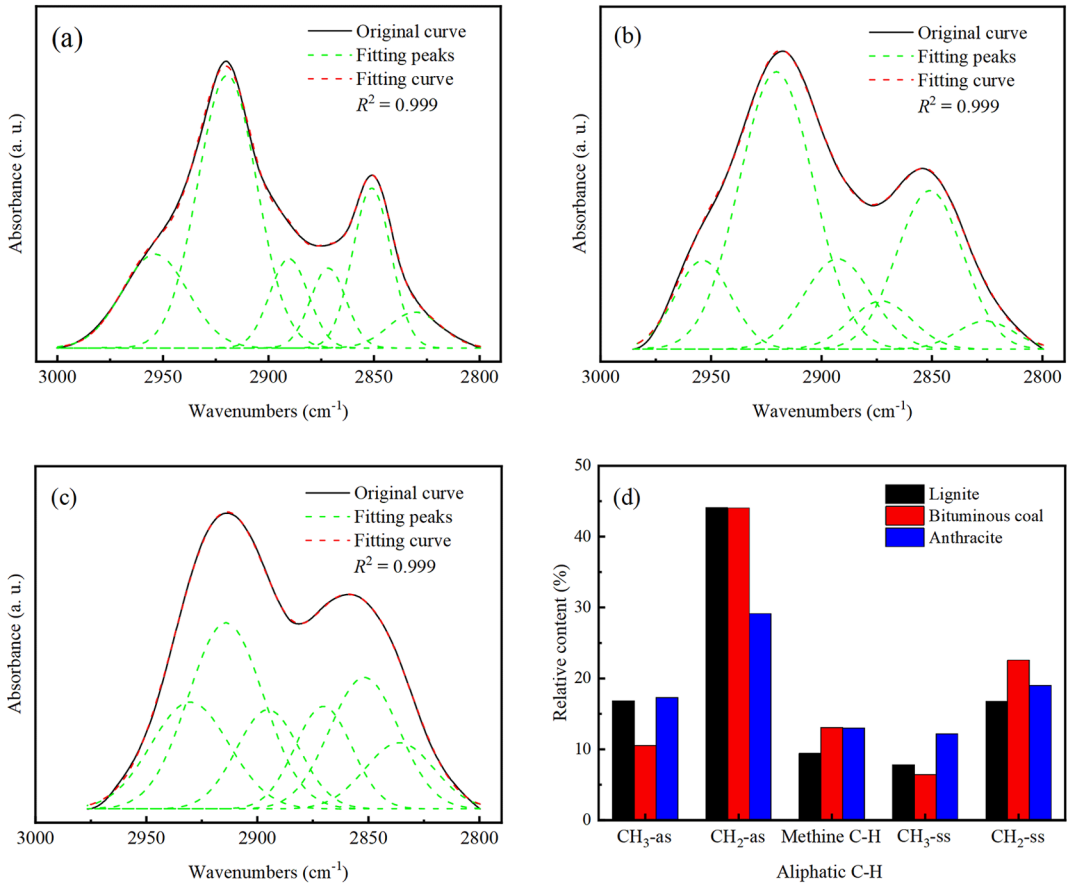

Figure 5. Curve-fitted FTIR spectra for the 3000−2800 cm^{-1} zone: (a) lignite, (b) bituminous coal, (c) anthracite, and (d) relative content.

where A_{2920} and A_{2950} correspond to the areas of the CH_2-as and CH_3-as peaks, respectively. The CH_2/CH_3 values of lignite, bituminous coal, and anthracite were 2.62, 4.19, and 1.69, respectively, indicating that the degree of branching of the aliphatic chain decreased during the conversion from lignite to bituminous coal, while the aliphatic chain significantly shortened during the conversion from bituminous coal to anthracite.

3.1.5. Hydrogen Bonds Involving Hydroxyl Groups. The υ mode of HBs involving −OH in coal can be divided into 5 types: free hydroxyl groups (O−H, 3750−3600 cm^{-1}), HBs formed by π electrons in the aromatic structures and hydroxyl groups (OH···π, 3525 cm^{-1}), self-associated HBs (OH···OH, 3420 cm^{-1}), HBs formed by O atoms in ethers and hydroxyl groups (OH···O, at 3300 cm^{-1}), and cyclic HBs formed by the hydrogen bonding of multiple −OH near 3200 cm^{-1}.[41,44]

Figure 6d shows the distribution of HBs in lignite, bituminous coal, and anthracite. Lignite exhibited the highest relative content of OH···OH bonds, whereas the lowest relative content was observed for free hydroxyl groups. This can be attributed to the presence of a significant number of −OH in lignite, which readily formed HBs with each other. On the other hand, bituminous coal and anthracite exhibited the highest relative content of OH···π bonds and the lowest relative content of cyclic HBs. These coals have numerous aromatic structures that promote the formation of HBs between the −OH and aromatic structures, while the formation of cyclic HBs among the −OH is less probable. During the conversion from lignite to bituminous coal, the decrease in the polar functional groups and the increase in the relative content of nonpolar aliphatic and aromatic structures resulted in a lower probability of hydrogen bonding between the −OH and polar functional groups. Consequently, the relative content of the free hydroxyl groups increased with the degree of coalification, while the relative content of OH···OH decreased. In contrast, during the conversion from bituminous coal to anthracite, the aromatic structures became significantly more abundant, leading to an increased likelihood of hydrogen bonding between the −OH and the π electrons in the aromatic structures. Furthermore, due to the accumulation of aromatic lamellae, the −OH could be positioned closer in space, resulting in an increase in the probability of OH···OH formation. Consequently, during the conversion from bituminous coal to anthracite, the relative content of OH···OH slightly increased. Bituminous coal can be characterized by the highest proportion of aliphatic structures (as shown in Figure 2) and the presence of longer aliphatic chains. Alcohols formed by linking long aliphatic chains may have a higher likelihood of creating OH···O bonds with ethers. Therefore, during the conversion from lignite to bituminous coal, the relative content of OH···O increased. However, during the conversion from bituminous coal to anthracite, the relative content of OH···O may decrease due to the significant reduction and shortening of the aliphatic chains and a decline in the relative content of R−OH.

3.2. XRD Analysis of Coal Samples. XRD was utilized to analyze the carbon structure of the coal samples. As shown in Figure 7, the (002) band corresponds to crystalline carbon, which is formed due to the condensation of aromatic rings and aliphatic rings and reflects the stacking characteristics of the

https://doi.org/10.1021/acsomega.3c08574
ACS Omega 2024, 9, 1881−1893

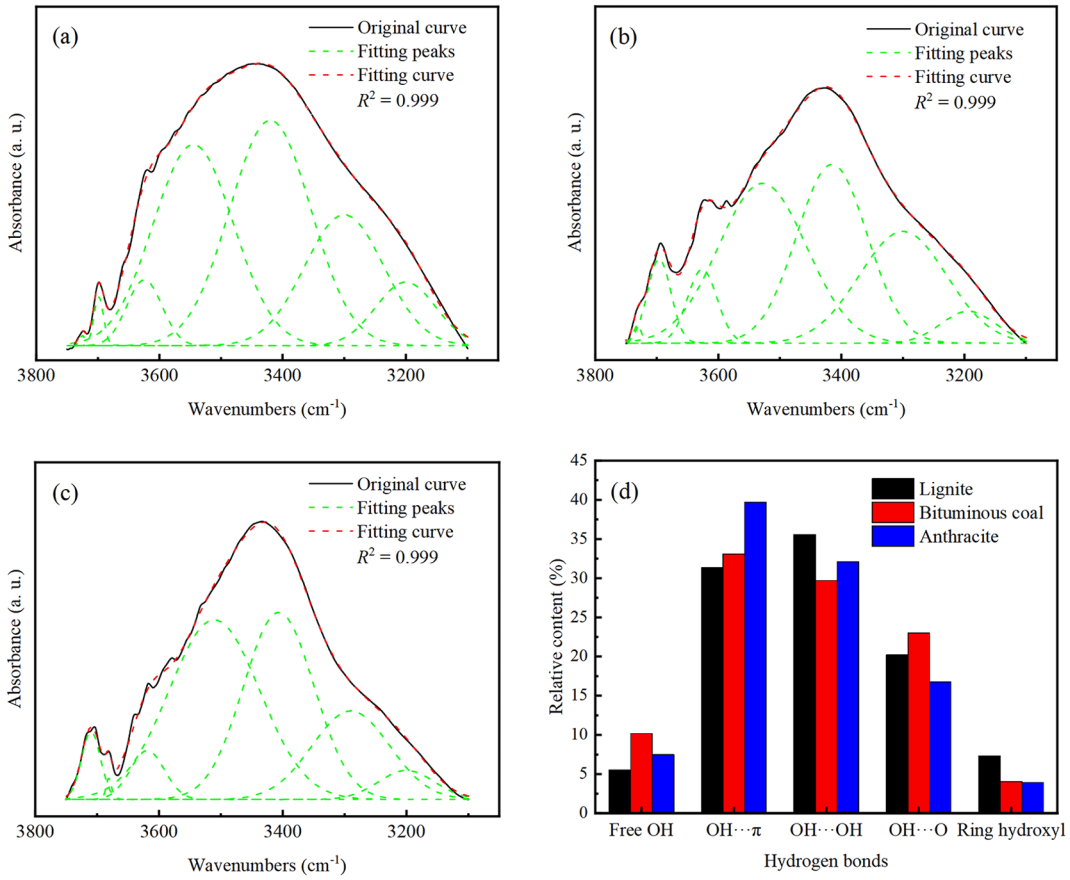

Figure 6. Curve-fitted FTIR spectra for the 3600−3100 cm^{-1} zone: (a) lignite, (b) bituminous coal, (c) anthracite, and (d) relative content.

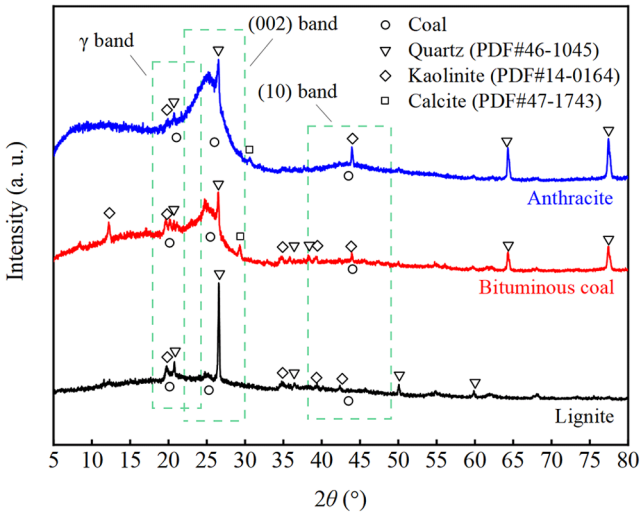

Figure 7. XRD spectra of lignite, bituminous coal, and anthracite.

aromatic layers; the γ band corresponds to amorphous carbon, which is composed of aliphatic chains grafted on the edges of the aromatic core; the (10) band characterizes the degree of condensation of the aromatic core (average diameter of the aromatic core).[15,19,45,46] The higher the degree of coalification, the sharper the (002) band, indicating an increase in the size of the aromatic core.

Figure 8 shows the peak fitting of the diffraction bands. By substituting the fitting result parameters into the Bragg and Scherrer equations (eqs 4−7), the average interlayer spacing (d_{002}), average stacking height (L_c), average diameter (L_a), and average number (N_{ave}) of the aromatic layers can be calculated.[19,45] In addition, the aromaticity (f_a) can be calculated using eq 8.[17,47]

$$d_{002} = \frac{\lambda}{2\sin(\pi\theta_{002}/180)} \quad (4)$$

$$L_c = \frac{180K_1\lambda}{\pi FWHM_{002}\cos(\pi\theta_{002}/180)} \quad (5)$$

$$L_a = \frac{180K_2\lambda}{\pi FWHM_{10}\cos(\pi\theta_{10}/180)} \quad (6)$$

$$N_{ave} = \frac{L_c}{d_{002}} + 1 \quad (7)$$

$$f_a = \frac{A_{002}}{A_{002} + A_\gamma} \quad (8)$$

where λ is the wavelength of the X-ray (0.154178 nm); θ_{002} and θ_{10} are the diffraction angles corresponding to the (002) and (10) bands (deg), respectively; $FWHM_{002}$ and $FWHM_{10}$ are the full width at half-maximum corresponding to the (002) and (10) bands (deg), respectively; K_1 and K_2 are constants, respectively taking values 0.89 and 1.84; and A_{002} and A_γ are the areas of the (002) and γ bands, respectively. Table 3 presents the calculation results of the carbon structures of the coal samples. Clearly, with the increase in the degree of coalification, the L_c, L_a, N_{ave}, and f_a values also increased. These findings suggest that the size of the aromatic core increased

https://doi.org/10.1021/acsomega.3c08574
ACS Omega 2024, 9, 1881−1893

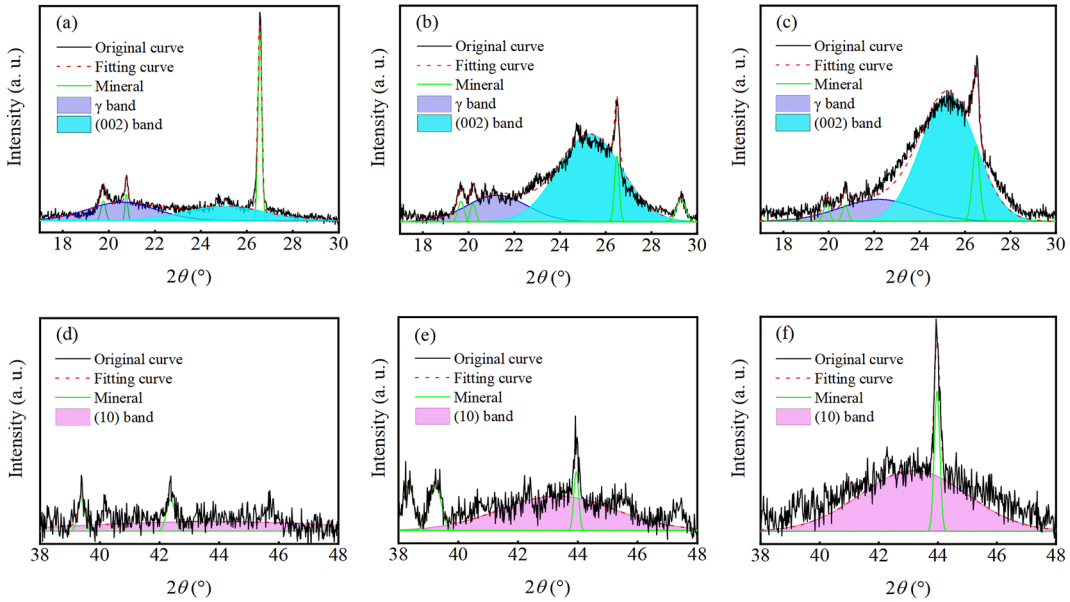

Figure 8. Curve-fitting XRD spectra of the coal samples: (a, d) lignite, (b, e) bituminous coal, and (c, f) anthracite.

Table 3. Carbon Structural Parameters Extracted from XRD Spectra

Coal	d_{002} (nm)	L_c (nm)	L_a (nm)	N_{ave} (layers)	f_a
Lignite	0.36	1.93	1.75	6.43	0.48
Bituminous coal	0.35	2.46	3.86	7.99	0.78
Anthracite	0.35	2.81	4.10	8.98	0.80

and that the ordering of the carbon structure in the coal intensified.

3.3. Coal Structure Models. Figure 9 shows the construction method of the structural models for lignite, bituminous coal, and anthracite. The number of aromatic rings (n) and their corresponding carbon atoms (C_{ar}), as well as the number of carbon atoms present in the side chains (C_{al}), were obtained by using the carbon structure parameters obtained from the XRD (as shown in Table 3). Furthermore, the form of the side chain was determined by using the aliphatic structure analysis results obtained from FTIR (as shown in Figure 5 and the CH_2/CH_3 parameter). To increase the model's convenience of application, reduce the construction

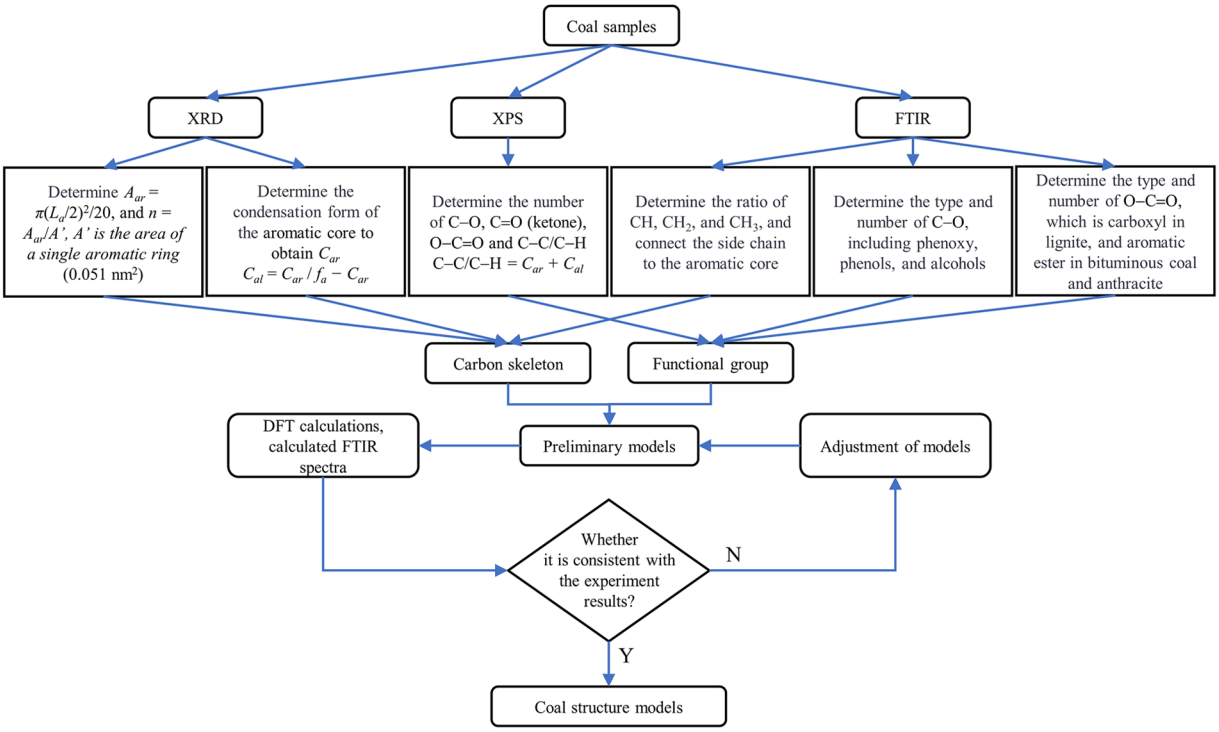

Figure 9. Flowchart of the model construction for the coal structure.

https://doi.org/10.1021/acsomega.3c08574
ACS Omega 2024, 9, 1881−1893

Table 4. Number of Functional Groups in Lignite, Bituminous Coal, and Anthracite

		C−C/C−H		C−O				
Coal	Carbon rings	C_{ar}	C_{al}	Phenoxy	Phenols	Alcohols	C═O	O−C═O
Lignite	2	12	13	1	1	3	1	1 (Carboxyl)
Bituminous coal	11	42	12	1	1	3	1	1 (Aryl esters)
Anthracite	13	43	11	2	3	1	1	1 (Aryl esters)

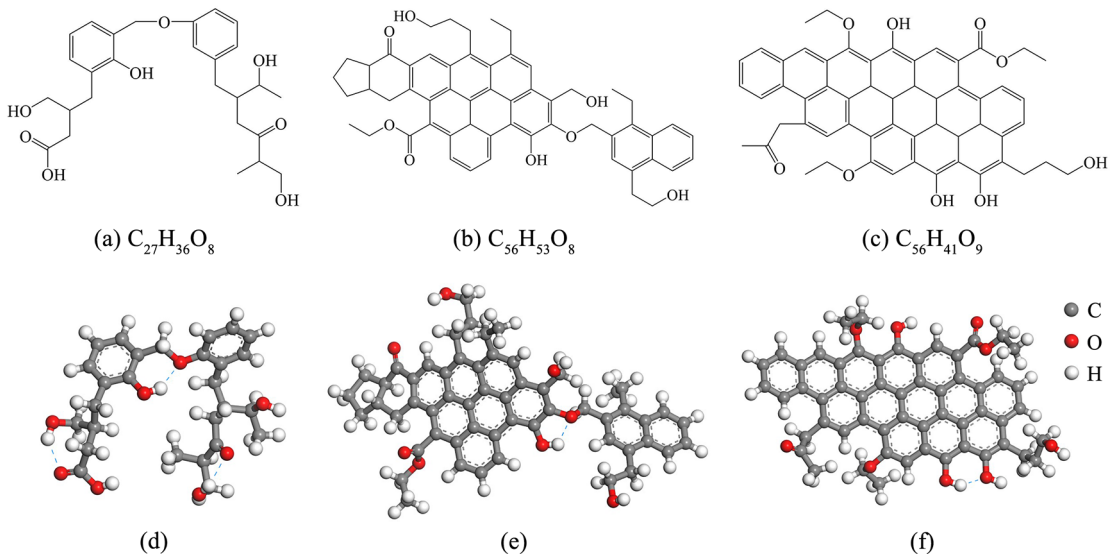

Figure 10. Structural formulas and geometrically optimized structure models of the coal samples: (a, d) lignite, (b, e) bituminous coal, amd (c, f) anthracite, where the blue dotted line indicates the HBs.

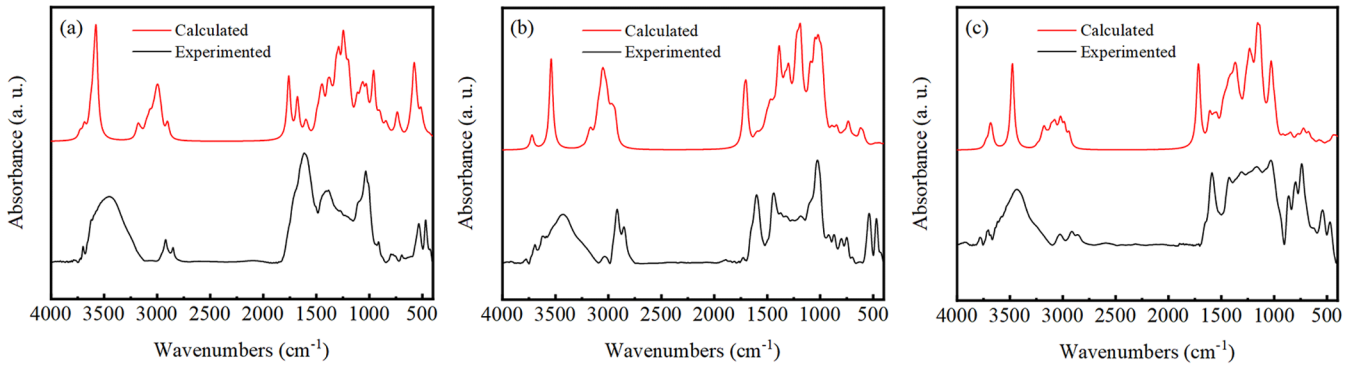

Figure 11. Experimental and calculated FTIR spectra of (a) lignite, (b) bituminous coal, and (c) anthracite.

workload, and ensure the model's representative nature, the equivalent circle area (A_{ar}) of the aromatic layer was reduced by 20 times. Finally, the specific types and quantities of the OFGs present in the coal samples were obtained using XPS (as shown in Figure 1) and FTIR analysis results of the OFGs (as shown in Figure 3 and Table 2). Since phenoxy and aromatic ethers mainly serve as connectors between the structural units, their quantity, which was calculated based on the proportion of FTIR analysis, would be approximately double the actual value. Therefore, the ratio of phenoxy was divided by 2. The elements N and S have little influence on the wettability of the coal, water molecule adsorption, and reagent adsorption, and therefore were not considered. Moreover, connecting side chains and functional groups on the aromatic core should be based on the content of the adjacent H atoms present in the aromatic structures (as shown in Figure 4). The calculated numerical values of the functional groups were rounded off, and if the value was less than 1 but greater than 0, it would be counted as 1. The calculated FTIR spectrum was compared with the experimental spectrum to allow the model to better reflect the chemical structure characteristics of the coal sample, and the model was revised continually to minimize discrepancies, resulting in an optimized model.

Table 4 presents the number of functional groups obtained using the above method. Figure 10 shows the obtained coal structure models. To confirm the precision of the coal structure models, the calculated FTIR spectra and experimental FTIR spectra were compared, as shown in Figure 11. The calculated spectrum was calculated from a single molecule in a vacuum, and its baseline was a horizontal straight line, while the baseline of the experimental spectrum was generally not a straight line. To facilitate a more intuitive comparison, the baseline of the experimental spectrum had been corrected. The shape of the aliphatic structure absorption bands (3000−

https://doi.org/10.1021/acsomega.3c08574
ACS Omega 2024, 9, 1881−1893

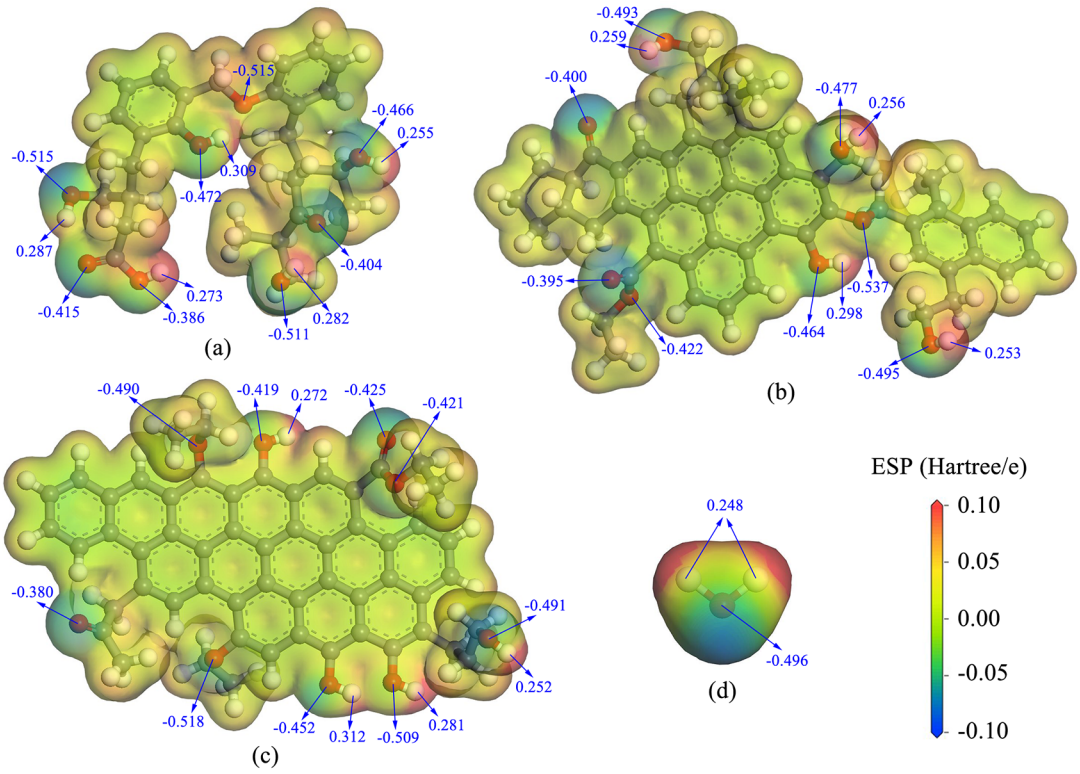

Figure 12. Mulliken charges and electrostatic potential (ESP) of coal structure models: (a) lignite, (b) bituminous coal, (c) anthracite, and (d) water molecule.

2800 cm^{-1}) in the calculated spectra was almost the same as that in the experimental spectra. The HB absorption bands (3600−3100 cm^{-1}) of the calculated spectra were narrower than the experimental spectra, with 1−2 sharp peaks. This result had also been observed in the studies conducted by Jia[48] and Qian[49] et al. This is because the calculated spectra were obtained from a single molecule, and the HBs were formed by intramolecular functional groups (three HBs were formed in the lignite structure model and one HB was formed in the bituminous coal and anthracite structure model, as shown in Figure 10d−f), without multiple molecular interactions. Therefore, the calculated spectra showed only free hydroxyl groups and a few types of HB peaks in this zone. During the construction of the structure models, the average size of the aromatic core was taken and reduced, resulting in fewer types of H atom substitutions on the aromatic ring in the models than in the actual coal samples. Therefore, the aromatic structure absorption bands (900−700 cm^{-1}) of the calculated spectra were weaker than that of the experimental spectra, with anthracite having the most significant difference. The shape of the absorption bands of the OFG (1800−1000 cm^{-1}) in the calculated spectra differed significantly from the experimental spectra due to the proportional reduction and simplification of the molecular weight of coal during the construction of the structure models, which considered only typical OFGs. Therefore, the types of OFGs in the structure models were fewer than in actual coal, resulting in a difference between the calculated and experimental absorption bands of the OFGs. In summary, the comparison results between the calculated and experimental FTIR spectra showed that the semiquantitative construction method based on the XRD, XPS, and FTIR analyses produces accurate and reliable coal structure models.

3.4. Application of the Models. Figure 12 shows the Mulliken charge (e) and electrostatic potential (ESP) of the coal structure models and the water molecule, where the electron density isosurface of the ESP map is 0.05 e/$Å^3$. The charge distribution plays a crucial role in intermolecular interactions (such as van der Waals forces, HBs, etc.) and can effectively describe and predict molecular adsorption and chemical reactions.[50−52] The charge distribution determines the electrophilicity and nucleophilicity of atoms. This means that the amount of positive or negative charges on an atom is directly related to its ability to accept or donate electrons.[53,54]

The presence of polar functional groups, predominantly OFGs, in the molecular structure of coal leads to an uneven distribution of electric charges on the coal surface. As shown in Figure 12, the electrostatic potential of the positive/negative charge is mainly concentrated around OFGs, with the local maximum negative value appearing around the O atom (blue region) and the local maximum positive value appearing around the H atom connected to the O atom (red region). In contrast, the electrostatic potential of the aromatic and aliphatic structures is approximately 0 hartree/e. Figure 12 shows the Mulliken charges (blue numbers) of these O and H atoms, with their positive and negative types and values being consistent with the electrostatic potential. Therefore, the O atoms in the OFGs have strong nucleophilicity, while the H atoms attached to the O atoms have strong electrophilicity. These atoms will become interaction sites for the water molecules. The H atoms of water molecules can form hydrogen bonds with O atoms of OFGs, while their O atoms can form hydrogen bonds with H atoms of OFGs.[30]

During the conversion from lignite to bituminous coal, the OFGs were significantly reduced (including the disappearance of carboxyls in bituminous coal), the relative content of the

https://doi.org/10.1021/acsomega.3c08574
ACS Omega 2024, 9, 1881−1893

aliphatic structure increased, and the degree of aromatic core condensation increased. Consequently, the area of local extreme regions of the positive/negative electrostatic potential on the surface of the coal molecules decreased significantly, leading to a substantial decrease in the number of interaction sites. Consequently, the wettability of the coal reduced significantly during this conversion process. During the conversion from bituminous coal to anthracite, the aliphatic chains became significantly shorter and the cycloalkanes underwent aromatization, resulting in a further increase in the condensation degree of the aromatic core. Meanwhile, there was a slight increase in the content of OFGs due to a decrease in the content of aliphatic structures and an increase in the contents of aromatic ether and phenolic hydroxyl groups. Therefore, the wettability slightly increased.

4. CONCLUSIONS

The chemical structure of coal changed regularly with an increase in the coalification degree. With the increase in the degree of coalification, there was a higher degree of H atom substitution in the aromatic ring, a higher condensation level, and increased size of the aromatic cores and an ordering of the carbon structure. During the conversion from lignite to bituminous coal, there was an increase in the content of aliphatic structures, and the aliphatic chains were cyclized. Additionally, there was a significant decrease in the content of OFGs, including the disappearance of carboxyl groups in bituminous coal. HBs involving −OH similarly decreased, while the content of free hydroxyl groups significantly increased. In the conversion from bituminous coal to anthracite, there was a substantial decrease in the content of aliphatic structures, the aliphatic chains became shorter, and the cycloalkanes underwent aromatization, while the content of OFGs slightly increased.

The semiquantitative construction method, which is based on XRD, XPS, and FTIR analyses, can provide accurate and reliable coal structure models. The calculated FTIR spectra of the structural models of lignite, bituminous coal, and anthracite were consistent with the experimental spectra. The absorption bands of the aliphatic structures showed the most consistency. These models successfully explained the differences in the wettability of the coal samples with varying coalification degrees. Lignite had the most OFGs and the largest area of local extreme regions of the electrostatic potential, resulting in the strongest wettability with water. Anthracite had slightly more OFGs than bituminous coal, giving it slightly stronger wettability to water than bituminous coal. The model construction method provides an approach to obtain a simplified model that can reflect the chemical structural characteristics of coal. The coal chemical structure model constructed in this study can be utilized as a universal model in molecular simulations to investigate various coal characteristics. However, these models did not include some relatively low content elements in coal, such as N and S. If these elements are required to be included in research, appropriate data (such as elemental analysis and XPS) may be supplemented, and related chemical structures can be added to these models.

AUTHOR INFORMATION

Corresponding Author

Chengyong Wang − *School of Mining and Mechanical Engineering, Liupanshui Normal University, Liupanshui 553004 Guizhou, China; Chinese National Engineering Research Center of Coal Preparation and Purification, China University of Mining and Technology, Xuzhou 221116 Jiangsu, China;* orcid.org/0000-0003-0771-4068; Email: wangchengyong87@163.com

Authors

Yaowen Xing − *Chinese National Engineering Research Center of Coal Preparation and Purification, China University of Mining and Technology, Xuzhou 221116 Jiangsu, China;* orcid.org/0000-0001-7930-4725

Kaiyi Shi − *School of Chemistry and Chemical Engineering, Qiannan Normal University for Nationalities, Duyun 558000 Guizhou, China;* orcid.org/0000-0001-9705-9022

Shiwei Wang − *School of Mining and Mechanical Engineering, Liupanshui Normal University, Liupanshui 553004 Guizhou, China;* orcid.org/0000-0002-3865-9658

Yangchao Xia − *Chinese National Engineering Research Center of Coal Preparation and Purification, China University of Mining and Technology, Xuzhou 221116 Jiangsu, China*

Jihui Li − *School of Chemical and Environmental Engineering, China University of Mining and Technology (Beijing), Beijing 100083, China;* orcid.org/0000-0002-4748-0692

Xiahui Gui − *Chinese National Engineering Research Center of Coal Preparation and Purification, China University of Mining and Technology, Xuzhou 221116 Jiangsu, China;* orcid.org/0000-0001-9270-7756

Complete contact information is available at: https://pubs.acs.org/10.1021/acsomega.3c08574

Funding

This work was supported by Guizhou Provincial Basic Research Program (Natural Science) (Qiankehejichu-ZK [2022] Yiban 532), Innovation Team Foundation of Education Department of Guizhou Province (qian jiao ji [2023]087), Academician Workstation of Liupanshui Normal University (Qiankehepingtairencai YSZ [2021]001), and Discipline Team of Liupanshui Normal University (LPSSY2023XKTD02).

Notes

The authors declare no competing financial interest.

ACKNOWLEDGMENTS

The authors would like to thank the shiyanjia lab (www.shiyanjia.com) for the FTIR test.

REFERENCES

(1) Murata, S.; Hosokawa, M.; Kidena, K.; Nomura, M. Analysis of oxygen-functional groups in brown coals. *Fuel Process. Technol.* **2000**, *67* (3), 231−243.

(2) Cheng, W.; Xue, J.; Xie, J.; Zhou, G.; Nie, W. A model of lignite macromolecular structures and its effect on the wettability of coal: A case study. *Energy Fuels* **2017**, *31* (12), 13834−13841.

(3) Dai, F.; Zhang, H. Quantitative study on the influence of the difference of the molecular structure on the spontaneous combustion characteristics of the coal metamorphism process. *Aip Adv.* **2021**, *11* (4), 045016.

(4) Hassid, A.; Klinger, M.; Krzack, S.; Cohen, H. TGA-DSC combined coal analysis as a tool for QC (quality control) and reactivity patterns of coals. *Acs Omega* **2022**, *7* (2), 1893−1907.

(5) Wu, D.; Zhang, W.; Fu, B.; Hu, G. Chemical structure and gas products of different rank coals during pyrolysis. *J. Therm. Anal. Calorim.* **2019**, *136* (5), 2017−2031.

https://doi.org/10.1021/acsomega.3c08574
ACS Omega 2024, 9, 1881−1893

(6) Xie, X.; Zhao, Y.; Qiu, P.; Lin, D.; Qian, J.; Hou, H.; Pei, J. Investigation of the relationship between infrared structure and pyrolysis reactivity of coals with different ranks. *Fuel* **2018**, *216*, 521−530.
(7) Liu, J.; Wang, M.; Liu, S.; Shangguan, J.; Yang, S. Cohesive components in coal and their cohesive mechanism during pyrolysis. *J. Anal Appl. Pyrol* **2023**, *170*, 105871.
(8) Shinn, J. H. From coal to single-stage and two-stage products: A reactive model of coal structure. *Fuel* **1984**, *63* (9), 1187−1196.
(9) Mathews, J. P.; Chaffee, A. L. The molecular representations of coal - A review. *Fuel* **2012**, *96*, 1−14.
(10) Given, P. H. Structure of bituminous coals: Evidence from distribution of hydrogen. *Nature* **1959**, *184* (4691), 980−981.
(11) Faulon, J. L.; Carlson, G. A.; Hatcher, P. G. A three-dimensional model for lignocellulose from gymnospermous wood. *Org. Geochem.* **1994**, *21* (12), 1169−1179.
(12) Faulon, J. L.; Carlson, G. A.; Hatcher, P. G. Statistical models for bituminous coal: a three-dimensional evaluation of structural and physical properties based on computer-generated structures. *Energy Fuels* **1993**, *7* (6), 1062−1072.
(13) Wender, I. Catalytic synthesis of chemicals from coal. *Catalysis Reviews* **1976**, *14* (1), 97−129.
(14) Wiser, W. H. *Conversion of bituminous coals to liquids and gases*; D. Reidel Publishing Company: 1984.
(15) Lu, L.; Sahajwalla, V.; Kong, C.; Harris, D. Quantitative X-ray diffraction analysis and its application to various coals. *Carbon* **2001**, *39* (12), 1821−1833.
(16) Mathews, J. P.; van Duin, A. C. T.; Chaffee, A. L. The utility of coal molecular models. *Fuel Process. Technol.* **2011**, *92* (4), 718−728.
(17) Wang, J.; He, Y.; Li, H.; Yu, J.; Xie, W.; Wei, H. The molecular structure of Inner Mongolia lignite utilizing XRD, solid state ^{13}C NMR, HRTEM and XPS techniques. *Fuel* **2017**, *203*, 764−773.
(18) Ibarra, J. V.; Muñoz, E.; Moliner, R. FTIR study of the evolution of coal structure during the coalification process. *Org. Geochem.* **1996**, *24* (6), 725−735.
(19) Okolo, G. N.; Neomagus, H. W. J. P.; Everson, R. C.; Roberts, M. J.; Bunt, J. R.; Sakurovs, R.; Mathews, J. P. Chemical-structural properties of South African bituminous coals: Insights from wide angle XRD-carbon fraction analysis, ATR-FTIR, solid state ^{13}C NMR, and HRTEM techniques. *Fuel* **2015**, *158* (2015), 779−792.
(20) Song, Y.; Feng, W.; Li, N.; Li, Y.; Zhi, K.; Teng, Y.; He, R.; Zhou, H.; Liu, Q. Effects of demineralization on the structure and combustion properties of Shengli lignite. *Fuel* **2016**, *183*, 659−667.
(21) Jiang, J.; Zhang, S.; Longhurst, P.; Yang, W.; Zheng, S. Molecular structure characterization of bituminous coal in Northern China via XRD, Raman and FTIR spectroscopy. *Spectrochimica Acta Part A: Molecular and Biomolecular Spectroscopy* **2021**, *255*, 119724.
(22) Kawashima, H.; Takanohashi, T. Modification of model structures of Upper Freeport coal extracts using ^{13}C NMR chemical shift calculations. *Energy Fuels* **2001**, *15* (3), 591−598.
(23) Feng, W.; Li, Z.; Gao, H.; Wang, Q.; Bai, H.; Li, P. Understanding the molecular structure of HSW coal at atomic level: A comprehensive characterization from combined experimental and computational study. *Green Energy & Environment* **2021**, *6* (1), 150−159.
(24) Wang, Q.; Zhang, J.; Li, H.; Zhang, H.; Bai, H.; Guo, Q. Exploring molecular structure characteristics and chemical index of Qinghua bituminous coal: A comprehensive insight from single molecule of macerals to particles with various sizes. *Powder Technol.* **2022**, *396*, 36−49.
(25) Guo, J.; Xia, Y.; Liu, Y.; Liu, S.; Zhang, L.; Li, B. Microscopic adsorption behaviors of ionic surfactants on lignite surface and its effect on the wettability of lignite: A simulation and experimental study. *J. Mol. Liq.* **2022**, *345*, 117851.
(26) Zhang, R.; Xing, Y.; Xia, Y.; Luo, J.; Tan, J.; Rong, G.; Gui, X. New insight into surface wetting of coal with varying coalification degree: An experimental and molecular dynamics simulation study. *Appl. Surf. Sci.* **2020**, *511*, 145610.
(27) Xia, Y.; Xing, Y.; Gui, X. Oily collector pre-dispersion for enhanced surface adsorption during fine low-rank coal flotation. *J. Ind. Eng. Chem.* **2020**, *82*, 303−308.
(28) Chen, J.; Min, F.-f.; Liu, L.-y. The interactions between fine particles of coal and kaolinite in aqueous, insights from experiments and molecular simulations. *Appl. Surf. Sci.* **2019**, *467−468*, 12−21.
(29) Zhao, Y.; Feng, Y.; Zhang, X. Molecular simulation of CO_2/CH_4 self- and transport diffusion coefficients in coal. *Fuel* **2016**, *165*, 19−27.
(30) Wang, C.; Xing, Y.; Xia, Y.; Zhang, R.; Wang, S.; Shi, K.; Tan, J.; Gui, X. Investigation of interactions between oxygen-containing groups and water molecules on coal surfaces using density functional theory. *Fuel* **2021**, *287*, 119556.
(31) Xi, X.; Jiang, S.; Zhang, W.; Wang, K.; Shao, H.; Wu, Z. An experimental study on the effect of ionic liquids on the structure and wetting characteristics of coal. *Fuel* **2019**, *244*, 176−183.
(32) Song, H.; Liu, G.; Zhang, J.; Wu, J. Pyrolysis characteristics and kinetics of low rank coals by TG-FTIR method. *Fuel Process. Technol.* **2017**, *156*, 454−460.
(33) Xu, C.; Wang, D.; Wang, H.; Xin, H.; Ma, L.; Zhu, X.; Zhang, Y.; Wang, Q. Effects of chemical properties of coal dust on its wettability. *Powder Technol.* **2017**, *318*, 33−39.
(34) Geng, W.; Nakajima, T.; Takanashi, H.; Ohki, A. Analysis of carboxyl group in coal and coal aromaticity by Fourier transform infrared (FT-IR) spectrometry. *Fuel* **2009**, *88* (1), 139−144.
(35) Sobkowiak, M.; Reisser, E.; Given, P.; Painter, P. Determination of aromatic and aliphatic CH groups in coal by FT-i.r.: 1. Studies of coal extracts. *Fuel* **1984**, *63* (9), 1245−1252.
(36) Saikia, B. K.; Boruah, R. K.; Gogoi, P. K. FT-IR and XRD analysis of coal from Makum coalfield of Assam. *Journal of Earth System Science* **2007**, *116* (6), 575−579.
(37) Xin, H.-h.; Wang, D.-m.; Qi, X.-y.; Qi, G.-s.; Dou, G.-l. Structural characteristics of coal functional groups using quantum chemistry for quantification of infrared spectra. *Fuel Process. Technol.* **2014**, *118*, 287−295.
(38) He, X.; Liu, X.; Nie, B.; Song, D. FTIR and Raman spectroscopy characterization of functional groups in various rank coals. *Fuel* **2017**, *206*, 555−563.
(39) Chen, Y.; Mastalerz, M.; Schimmelmann, A. Characterization of chemical functional groups in macerals across different coal ranks via micro-FTIR spectroscopy. *International Journal of Coal Geology* **2012**, *104*, 22−33.
(40) Zhang, Y.; Zhang, X.; Hu, S. Structural transformations of coal at low temperature oxidation via in-situ FTIR. *Combust. Sci. Technol.* **2021**, *193* (11), 1885−1902.
(41) Yao, J.; Ji, H.; Lu, H.; Gao, T. Effect of tetrahydrofuran extraction on surface functional groups of coking coal and its wettability. *J. Anal Methods Chem.* **2019**, *2019*, 1285462.
(42) Yao, S.; Zhang, K.; Jiao, K.; Hu, W. Evolution of coal structures: FTIR analyses of experimental simulations and naturally matured coals in the Ordos Basin, China. *Energ Explor Exploit* **2011**, *29* (1), 1−19.
(43) Ibarra, J. V.; Moliner, R.; Bonet, A. J. FT-i.r. investigation on char formation during the early stages of coal pyrolysis. *Fuel* **1994**, *73* (6), 918−924.
(44) Painter, P. C.; Sobkowiak, M.; Youtcheff, J. FT-i.r. study of hydrogen bonding in coal. *Fuel* **1987**, *66* (7), 973−978.
(45) Neupane, B.; Ju, Y.; Silwal, B. R.; Singh, P. K.; Huang, C. Structural investigations of Eocene coals from foreland basin of central Nepal Himalaya. *Energ Explor Exploit* **2017**, *35* (6), 713−733.
(46) Wang, C.; Xing, Y.; Lei, Y.; Xia, Y.; Zhang, C.; Zhang, R.; Wang, S.; Chen, P.; Zhu, S.; Li, J.; et al. Adsorption of water on carbon materials: The formation of "water bridge" and its effect on water adsorption. *Colloids Surf., A* **2021**, *631*, 127719.
(47) Sonibare, O. O.; Haeger, T.; Foley, S. F. Structural characterization of Nigerian coals by X-ray diffraction, Raman and FTIR spectroscopy. *Energy* **2010**, *35* (12), 5347−5353.
(48) Jia, J.-b.; Wang, Y.; Li, F.-H.; Yi, G.-Y.; Zeng, F.-G.; Guo, H.-Y. IR spectrum simulation of molecular structure model of Shendong

https://doi.org/10.1021/acsomega.3c08574
ACS Omega 2024, 9, 1881−1893

coal vitrinite by using quantum chemistry method. *Spectrosc Spect Anal* **2014**, *34* (1), 47−51.
(49) Qian, L.; Tao, C.; Ma, C.; Xue, J.; Guo, F.; Jia, X.; Yan, W. Construction of a macromolecular structure model for Zhundong subbituminous coal. *J. Mol. Struct.* **2022**, *1248*, 131496.
(50) Israelachvili, J. N. *Intermolecular and surface forces*, 3rd ed.; Academic Press: 2011.
(51) Gao, Z.; Ding, Y.; Yang, W.; Han, W. DFT study of water adsorption on lignite molecule surface. *J. Mol. Model* **2017**, *23* (1), 27.
(52) He, Q.; Xiao, Y.; Miao, Z.; Sun, M.; Wan, K.; Gao, M. Water clusters in lignite and desorption energy calculation by density functional theory. *Acs Omega* **2019**, *4* (10), 14219−14225.
(53) Wang, B.; Rong, C.; Chattaraj, P. K.; Liu, S. A comparative study to predict regioselectivity, electrophilicity and nucleophilicity with Fukui function and Hirshfeld charge. *Theor. Chem. Acc.* **2019**, *138* (12), 124.
(54) Oña, O. B.; De Clercq, O.; Alcoba, D. R.; Torre, A.; Lain, L.; Van Neck, D.; Bultinck, P. Atom and bond Fukui functions and matrices: A Hirshfeld-I atoms-in-molecule approach. *ChemPhysChem* **2016**, *17* (18), 2881−2889.

https://doi.org/10.1021/acsomega.3c08574
ACS Omega 2024, 9, 1881−1893